Digital Communications and Networks 7 (2021) 605–614

Contents lists available at ScienceDirect

Digital Communications and Networks

journal homepage: www.keaipublishing.com/dcan

Petahertz communication: Harmonizing optical spectra for wireless communications

Zhengyuan Xu [a], Weijie Liu [a], Zhaocheng Wang [b,*], Lajos Hanzo [c]

[a] Wireless-Optical Communications Key Laboratory of CAS, University of Science and Technology of China, Hefei, 230027, China
[b] Department of Electronic Engineering, Tsinghua University, Beijing, 100084, China
[c] School of Electronics and Computer Science, University of Southampton, Southampton, SO17 1BJ, UK

ARTICLE INFO

Keywords:
Petahertz communication
Petahertz spectrum harmonization
Optical spectrum
Optical wireless communication

ABSTRACT

With the rapid deployment of Next-Generation Networks (NGN), the research community has initiated discussions on an entirely new suite of optical enabling techniques. To pave the way for the development of future wireless networks, this article aims to unify the existing infrared, visible light, and ultraviolet subbands while also exploring the potential of the Petahertz (PHz) band to support extremely bandwidth-thirsty telepresence style applications. Our focus is on the emerging Petahertz Communication (PetaCom) framework, scenario-dependent propagation channels, modulation schemes, system performance, multiple access techniques, and networking. We conclude with a range of PetaCom challenges and open research issues.

1. Introduction

In the past four decades, four wireless generations have emerged [1]. The recent development and roll-out of the Fifth-Generation (5G) wireless communication standard supports three fundamentally different services: enhanced Mobile Broadband (eMBB), massive Machine-Type Communications (mMTC), and ultra-Reliable Low-Latency Communications (uRLLC). These application scenarios will ultimately change the way people and "things" are connected. Evolution continues towards Sixth-Generation (6G) wireless systems to further improve data rates, connection density, and latency [2–4]. The emerging and increasingly sophisticated enabling technologies aim to meet the tight requirements that support flawless telepresence applications, such as immersive high-definition Extended Reality (XR) [5], Virtual Reality (VR), Augmented Reality (AR), and Mixed Reality (MR). Supporting HD holographic videos and digital twins [4] requires tremendous bandwidth.

In attempting to satisfy the aforementioned demanding requirements, the quest for unused bandwidths has gradually led to increasing carrier frequencies from 450 MHz to 60 GHz Millimeter-Wave (mmW) frequencies and even to Terahertz (THz) [3]. The success of mmW solutions critically hinges on the development of high-gain integrated Transmitter (Tx) and Receiver (Rx) arrays. These solutions partially alleviate the pressing need for increased capacity but at the cost of high power consumption and complexity. The THz band, which is widely used in imaging, offers tremendous bandwidth potential, but available devices still lack maturity at the time of writing. In addition, these bands impose high path loss, necessitating high-gain beamforming to compensate. As the frequency increases, the electromagnetic wave undergoes a transfiguration, where the mmW and THz spectra straddle the Radio Frequency (RF) and optical bands along the wavelength/frequency axis. In this context, Optical Wireless Communication (OWC) technologies are expected to serve as beneficial complementary candidate solutions for future wireless networks [6].

This article will propose a unified framework to harmonize the existing segmented optical subbands from the wireless communication perspectives. It will also discuss detailed harmonization approaches from devices to systems and networks.

2. Petahertz spectrum and communication

The hitherto scarcely-used unlicensed spectral band is the Petahertz (PHz) band with a frequency ranging from 0.01 PHz to 100 PHz, where 1 PHz = 10^{15} Hz. The corresponding wavelength, which is usually convenient to use in OWC, spans from 30 μm to 3 nm, as shown in Fig. 1.

The PHz band harmonizes existing Infrared (IR), Visible Light (VL), and Ultraviolet (UV) subbands although there is no clear boundary between IR and THz bands or UV and X-ray bands. OWC systems focus primarily on an environment-dependent frequency range of 0.2–1.5 PHz

* Corresponding author.
E-mail addresses: xuzy@ustc.edu.cn (Z. Xu), lwj1993@mail.ustc.edu.cn (W. Liu), zcwang@tsinghua.edu.cn (Z. Wang), lh@ecs.soton.ac.uk (L. Hanzo).

https://doi.org/10.1016/j.dcan.2021.08.001
Received 20 April 2021; Received in revised form 22 July 2021; Accepted 2 August 2021
Available online 6 August 2021

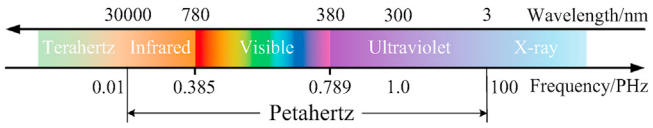

Fig. 1. Petahertz spectrum and its constituents adjacent to Terahertz and X-ray.

or a similar wavelength range of 0.2–1.5 μm [6].

According to the application scenarios and carrier subbands, traditional OWC systems may be roughly divided into the following types [6]: UV, VL, IR, or Free-Space Optical (FSO) communications. The IEEE Std 802.15.7–2018 [7], the latest revision of the standard on Visible Light Communication (VLC), defines OWC in terms of the optical light wavelengths spanning from 190 nm to 10 μm. The wavelengths are divided into eight bands, with the main focus being on six VL bands, in which data rates below 100 Mbps are specified for six different physical layer (PHY) operational modes.

In UV communication, the UV-C subband of 200–280 nm is "solar-blind" near the earth's surface due to the ozone layer's absorption in the upper atmosphere. Thus, a photon detector can perform photon-counting quantum detection, despite solar radiation [8]. Furthermore, suspended particles serve as tiny relay stations, which enable Non-Line-Of-Sight (NLOS) communication via strong scattering. Terrestrial terminals can employ wide Field-Of-View (FOV) Rxs to increase the Signal-to-Noise Ratio (SNR). The NLOS propagation is beneficial for mitigating the pointing error of Line-Of-Sight (LOS) Transceivers (Tx/Rxs). Low-power and low-cost UV systems are readily implementable using off-the-shelf devices, such as Light-Emitting Diodes (LEDs), allowing safe radiation levels for humans. Naturally, this requires satisfying the wavelength-dependent maximum exposure limits, such as 3 mJ/cm^2 at 270 nm within 1 s [8], to protect human eyes and skin. However, mMTC does not require strict exposure protection.

VLC operates in the VL subband of 380–780 nm, which is the most active OWC research area [1]. It uses lighting LEDs for its Txs to achieve concurrent lighting/display and high-speed data transmission in indoor settings. In duality with WiFi, VLC is generalized as Light-Fidelity (LiFi) to describe a complete bi-directional multiuser wireless system built upon LED lighting infrastructure [9]. VLC can also be extended to outdoor vehicular networking after carefully considering Tx/Rx mobility, beam divergence, and surrounding reflected light [10,11].

In IR communication, a fraction of the IR subband at 780–950 nm behaves similarly to VL but has different emission levels under stricter radiation safety regulations. A comprehensive description of indoor LOS and reflected/diffused NLOS IR channels, Tx/Rx designs, and local-area networks has been provided in Ref. [12]. IR light has a limited transmission distance under its power exposure limit. Thus, IR communication is confined within a room and generally has small cells with a radius of less than a few meters.

Table 1
Comparisons among wireless technologies.

Wireless Technology	mmWave	Terahertz	Petahertz
Frequency Range	30–300 GHz	0.1–10 THz	0.01–100 PHz
Typical Data Rate	~ 10 Gbps	~ 1 Tbps	~ 100 Tbps
Network Coverage	Small/Medium	Small/ Medium	Large
Infrastructure Cost	High	High	Medium
EMI	High	Medium	Low
Security	Medium	High	High
Propagation	Indoor/ Outdoor	Indoor/ Outdoor	Indoor/Outdoor/ Underwater
Positioning Accuracy	Low	Medium	Medium/High
Sensing/Imaging	Yes	Yes	Yes
Lighting/Display	No	No	Yes

FSO communication is fundamentally based on transmitting data-modulated IR light with a high-power laser through space, collecting the optical signal with a large telescope [6]. It offers wavelength-division aided full-duplex transmission at high data rates. Its spatial, temporal, wavelength and polarization diversities are exploitable to compensate for the geometric loss, atmospheric loss, and turbulence-induced fading [13,14] experienced when communicating among terrestrial terminals, ground stations, and flying platforms.

Compared to existing mmW and THz wireless technologies, PHz technologies enjoy several unique characteristics and advantages. Table 1 and the remainder of this section present some of the major comparative aspects in communication, positioning, and other functions.

First, PHz technologies offer bandwidth increases that are orders of magnitude higher (over 1 PHz) to deliver a much higher data rate (tens of Terabits per second (Tbps) or more) to support the so-called vertical industries and society as a whole, which rely on high-definition videos for telepresence [3]. Such a rate is feasible in free space and has also been demonstrated in optical fiber communications.

Second, existing low-cost optical devices that have been widely adopted by ubiquitous lighting, display, and imaging, can be retrofitted as Txs and Rxs. Together with specialized communication light sources, they facilitate large-scale network coverage and long-range communication indoors, outdoors, underwater, and in deep space. The ubiquitous lighting and optical monitoring infrastructures assist in supporting the Internet of Things (IoT).

Third, the PHz wave imposes no Electromagnetic Interference (EMI) and is not affected by existing RF-based carriers. It can also operate in harsh or RF-restrictive environments. Hence, it is ideal for industrial manufacturing environments, medical spaces, explosives warehouses, and underwater scenarios.

Fourth, the PHz spectrum is consistent with the human-friendly daylight solar radiation spectrum. The spectrum may be the only higher-frequency spectrum sufficiently suitable for human communications, while the X-ray spectrum is only acceptable for machines, such as those operating in deep space.

Lastly, the PHz beamwidth is easily controlled at milliradian (mrad) or microradian (μrad) levels. The narrowly focused beam leads to low geometric propagation loss, compensating for channel attenuation loss. It also allows denser spatial reuse, hence yielding increased area spectral efficiency and enhanced data security. The beamwidth's directivity and short-wavelength also enable high-resolution six-Dimensional (6D) positioning, including spatial location and angular orientation, to facilitate accurate sensing and controlling of mobile terminals and nodes. In addition to positioning, the PHz spectrum is applicable to functions beyond communication, such as sensing, imaging, lighting, and display.

However, the Petahertz wireless technologies suffer from ambient environmental interference emitted by objects and biological bodies that radiate Petahertz waves. Interfering PHz sources include sunlight, moonlight, artificial lights, human bodies, fluorescent organisms in the atmosphere, and marine environments. Therefore, bespoke interference mitigation techniques have to be designed to enhance system resilience. Meanwhile, fragmented utilization of the Petahertz spectrum hinders the realization of its full potential in wireless communications.

3. Harmonization and Petahertz communication

This section will elaborate on why and how Petahertz spectrum harmonization will be achieved from different perspectives within the PHz spectrum.

3.1. Reasons for harmonization

At the time of writing, the PHz spectrum is under fragmented utilization. To fully realize its potential, the Petahertz Communication (PetaCom) framework is capable of overcoming current spectrum segmentation by harmonizing existing segmented UV-VL-IR subbands for

wireless communication with any PHz carrier. This integration is strongly motivated by the following reasons.

First, traditional classification into the UV-VL-IR subbands is based on the human eye's spectral sensitivity to VL. However, conventional VLC applications may be readily extended to wireless communications. Naturally, VLC is also suitable for machines, as in mMTC [2]. These terminals may be equipped with optical sensors potentially activated by either visible or invisible light. The advocated PetaCom framework intrinsically amalgamates the entire PHz spectrum, as will be discussed in Sec. 3.2. Proposed spectrum sharing and aggregation ideas for long-term evolution and WiFi frequency bands [15] can be followed to improve PHz spectrum exploitation.

Second, to enhance the PetaCom framework's adaptability to diverse environments, it is essential to scan the entire PHz spectrum and find the most suitable carrier to match the specific signal propagation characteristics encountered. Possible PetaCom scenarios in future wireless sectors are depicted in Fig. 2. PetaCom may be expected to become a key enabler for small-to large-scale networks operating in three-dimensional space. It is capable of supporting high-speed interaction among various indoor and outdoor traditional/emerging terminals, including smartphones, laptops, robots, vehicles, underwater communications between divers and Unmanned Aerial Vehicles (UAVs), free-space communications among flying terminals (such as UAVs, drones, aircraft, balloons, and space satellites), ground communications, and space-air-water communications.

Third, some communicating parties and applications are cautious when selecting optical information carriers, given particular biological safety or information security constraints. Fortunately, the PHz spectrum can provide a large set of carrier options. For example, humans as communicating parties prefer to opt for a specific spectral segment such as VL to avoid radiation exposure and ensure safety [6]. The information security demanded during battlefield situations is satisfied by the low probability of interception offered by a UV subband [8]. Alternatively, wavelength tuning within a suitable PHz segment is another excellent security choice, as exemplified by frequency hopping in radio communication.

We advocate unified and coherently aggregated PHz wavelength regions to provide seamless services. For example, a standalone indoor VLC system can hardly achieve full duplexing, even for a single link, but it is conveniently complemented by other carrier bands, such as IR and WiFi, to form an aggregated/hybrid full-duplex system. Several use cases exploiting the associated PHz spectrum can be envisioned. Table 2 illustrates some typical use cases and candidate spectra in different scenarios. They include indoor home and office wireless access networks, enterprise networks [16,17], satellite networks [14, 18], and Internet of Underwater Things (IoUT) [19,20].

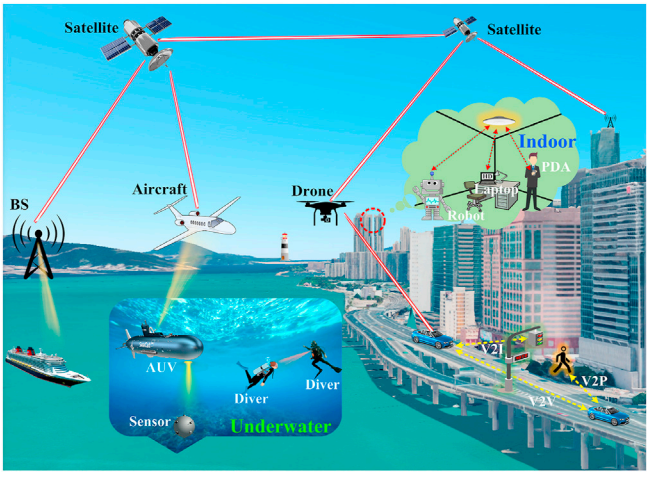

Fig. 2. Envisioned indoor, outdoor terrestrial, space, and underwater PetaCom scenarios.

Table 2
Petahertz use cases and candidate spectra.

Use Cases	Candidate Spectrum
Indoor Wireless	850–1550 nm uplink 380–780 nm downlink
Immersive XR	850–1550 nm
Mobile Hologram	380–780 nm
Industrial Network	250–1550 nm
Vehicular Network	250–1550 nm
Mobile Backhaul	850–1550 nm
Satellite Network	850–1550 nm
Underwater Internet	350–650 nm
Vertical above Earth	250–280 nm 850–1550 nm

3.2. Petahertz communication framework

A PetaCom network may assume diverse topologies where multiple nodes engage in decentralized communication or centralized communication with a central node. Extensive aspects of PHz spectrum harmonization need to be described within the PetaCom framework. Fig. 3 depicts the framework from a link-level communication perspective, while its networking level counterpart will be highlighted in the last part of this Section. In the link-level framework, two nodes communicate through a PHz channel. Each node is equipped with a Tx/Rx consisting of a channel sensing unit, a PHz device aggregation unit, and a communication unit.

The channel sensing unit of Fig. 3 first scans a predefined PHz spectrum of a continuous wavelength range $\Pi = [\lambda_L, \lambda_H]$, where λ_L and λ_H represent the lowest and highest wavelengths, respectively. Some parts of the spectrum are occupied by other active nodes within the same geographic area. After skipping the interfering channels, the available channels are grouped into a wavelength subset $\Phi = \{\lambda_1, \ldots, \lambda_K, \Pi_1, \ldots, \Pi_N\}$, which consists of K discrete wavelengths $\lambda_1, \ldots, \lambda_K$ and N continuous wavelength subbands $\Pi_1, \ldots, \Pi_N$, where $\Pi_i = [\lambda_{iL}, \lambda_{iH}]$ for $i = 1, \ldots, N$. In the available channel subset Φ, there are also k_0 wavelengths and n_0 subbands exhibiting excessive channel attenuation, or having radiation safety and information security problems. After these wavelengths and subbands are excluded, the remaining channels are arranged into a qualified channel subset $\mathcal{S} = \Phi \setminus \{\lambda_1, \ldots, \lambda_{k_0}, \Pi_1, \ldots, \Pi_{n_0}\} = \{\lambda_{k_0+1}, \ldots, \lambda_K, \Pi_{n_0+1}, \ldots, \Pi_N\}$, where $\setminus$ represents the element removal operation.

The channel sensing results are fed to the PHz device aggregation unit of Fig. 3 to activate the relevant PHz sources and detectors for communication through a PHz channel. The framework's communication unit then performs digital and analog signal processing that includes, but is not limited to, modulation/demodulation, signal pre-/post-processing, estimation, and detection. The PHz channel shown in Fig. 3 represents the signal propagation environment encountered.

In addition to the associated channel sensing, device, communication, and channel aspects of node-to-node communication, the unified PetaCom framework also covers harmonization from system- and network-oriented perspectives when multiple nodes are connected to the network. Therefore, the PetaCom devices, channel characterization, modulation, system performance evaluation, multiple access, and

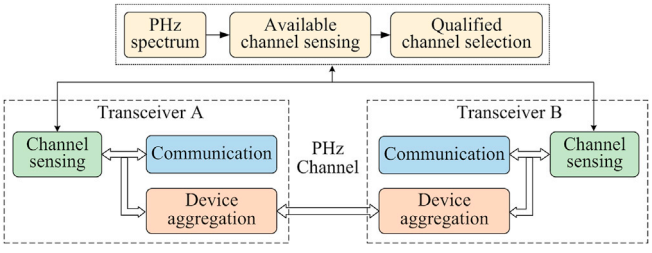

Fig. 3. Link-level PetaCom framework.

networking are all coherently integrated across the entire PHz spectrum, as detailed in Subsections 3.3 to 3.7.

3.3. PetaCom device

From a device perspective, there are different ways for a Tx/Rx to match the qualified channel set $\mathcal{S}$. A PetaCom emitter with coherent, partially coherent, or non-coherent light sources at the Tx may generate carriers in the form of a single wavelength, multiple distinct wavelengths, scattered segments, or even a whole continuous chunk of wavelengths in the spectrum, as described in Sec. 3.2. Accordingly, a monochromatic laser with a fixed wavelength (e.g., 525 nm for underwater communication or 905 nm for atmospheric communication) can be utilized. Alternatively, an array of multiple lasers operating at different wavelengths can be activated jointly or selectively using element switching. In some cases, a single emitter may occupy a wide range of spectra, as exemplified by a white LED in the wavelength range of 380–780 nm. Exploiting an entire chunk of the spectrum is also realizable using a monochromatic but tunable laser, whose wavelength varies continuously with the electric driving current. When multiple LEDs centered at different wavelengths are integrated, such as a set of R/G/B LEDs, the carrier is constituted by segmented spectra. The best wavelengths to be used can be found by agile resource-allocation relying on suitable optical field control to match both the emitters and the channel characteristics.

At the data-recovery Rx of the same node, the wavelength or band is selected by an appropriate optical filter and photodetector. The photodetector may assume different forms, such as a Photodiode (PD), Avalanche Photodiode (APD), Single-Photon Avalanche Detector (SPAD), Photomultiplier Tube (PMT), or Complementary Metal Oxide Semiconductor (CMOS) image sensor. The SPAD and PMT are powerful at detecting extremely weak optical signals, down to single photons. The resultant photon counting techniques are applicable in severe channel attenuation scenarios [21,22], such as scattering, shadowing, partial blockage, dimming, or long-distance communication. The optical cameras embedded in smartphones may readily serve as optical detectors, as in Optical Camera Communication (OCC) [23–25].

The wide spectral sensitivity of the PHz sources and detectors will offer a new horizon for the adaptation of a PetaCom Tx/Rx. Although some barriers exist for devices operating across a wide wavelength range, some successful cross-band trials have been demonstrated by diverse devices (e.g., UV excited VL lighting LEDs upon white phosphor [26], IR-VL-UV spectrometers [27]). These off-the-shelf devices offer valuable insight and promising solutions for PHz communication device fabrication and operations.

3.4. PetaCom channel modeling and characterization

In quantum mechanics, an electromagnetic wave exhibits both wave-like and particle-like properties, termed the wave-particle duality. A wavelength-dependent PetaCom channel, either classical or quantum [1], can be conveniently described across PHz wavelengths either at the continuous waveform level or the discrete photon level. It obeys all the wave or photon propagation laws of absorption, scattering, reflection, and turbulence. The particle property becomes more evident as light intensity is reduced by channel attenuation or intentional power-reduction in quantum communication. In such cases, photon tracing is useful for describing photon trajectory and reception probability. Therefore, the wave and particle manifestations and their state transitions constitute the most representative states, characterized in 3D space and wavelength dimensions. In addition to experimentation, one may adopt transport theory, ray-tracing analysis, and Monte Carlo simulation to study the wave propagation behaviors in power attenuation, multipath propagation, and turbulence, which would be leveraged in associated Tx/Rx design. For example, channel path loss across the 200–1600 nm wavelength range was simulated under different particle densities, particle size, communication distance, and visibility conditions [28].

3.4.1. Indoor channel

Indoor PetaCom requires a high SNR for achieving a high data rate. Therefore, LOS paths are expected for most applications, while supplemental NLOS paths are created by object reflection and diffusion. Generally, an indoor channel consists of a direct LOS path plus some high-order reflected and diffused NLOS paths [12,29]. The LOS geometric loss due to beam-divergence is predictable, given the source radiation pattern, link geometry, and aperture size of the Rx. Multipath reflections cause temporal spreading and lead to Inter-Symbol Interference (ISI), where usually only the first-order reflection is non-negligible. Diffused paths occur when the Tx is directed towards the ceiling or walls. In contrast to RF, the PHz wave suffers from shadowing due to potential random movements and blockage, which can be alleviated by adjusting the Tx/Rx orientation.

3.4.2. Outdoor channel

The outdoor PHz wave is significantly attenuated by atmospheric propagation phenomena through absorption, scattering, and turbulence. It can be analyzed by the software tool MODTRAN [14]. The blue curve in Fig. 4a shows the attenuation evaluated by simulation at frequencies of 0.01–1.5 PHz after horizontal propagation over a distance of 1 km near the ground under maximum visibility of 25 km. The red curve represents typical solar radiance. For PetaCom, one can set the signal attenuation threshold below 3 dB to find the best transmission windows, as listed in Table 3. Alternatively, one can aim for minimizing the solar background radiation, such as below 50 $\mu W/cm^2/nm$ corresponding to the band beyond 0.25–1.0 PHz. Above 1.0 PHz, the strong forward-scattering contributes to severe attenuation, and the LOS transmission distance is limited to the order of 10 km. The NLOS channel mainly relies on scattering via suspended molecules and aerosols [30,31].

Under clear conditions, solar heating and wind create both temperature and atmospheric pressure inhomogeneity, leading to atmospheric turbulence [32,33]. Several fading channel models have been developed for FSO systems [13,14]. The lognormal model is most widely accepted under weak turbulence, while the Gamma-Gamma model is more accurate for strong turbulence. For a vertical space-ground link [14], the Hufnagel-Valley model is used for characterizing turbulence as a function of altitude. In particular, the particle density, temperature, and pressure vary with altitude, resulting in layered transmission media and inhomogeneity to be integrated into future wave propagation studies.

The rain and snow significantly affect the signal propagation in certain PHz wavelength regions [34]. Rain attenuation is typically modeled by the power law with rain precipitation intensity, which is generally independent of the wavelength because raindrops have a larger size than the wavelength [35]. However, the cross-sectional area of snowflakes is larger than that of raindrops, making snow attenuation higher than that of rain at the same precipitation rate [36]. Various outdoor attenuation models have been developed and reported [14,37,38], ranging from the UV to the far IR band within the PHz spectrum in the presence of aerosols, clouds, and precipitation.

3.4.3. Underwater channel

The underwater channel characteristics depend on the optical properties of different water types, which are categorized according to their turbidity and attenuation effects: Type I - extremely clear oceanic waters, Type II - clear coastal waters, and Type III - fairly turbid waters [39]. Fig. 4b shows the simulated water attenuation, assuming light propagation through 10 m and 100 m, following the Beer-Lambert law, and using the corresponding extinction coefficients at UV/VL wavelengths of 310–700 nm in the aforementioned water-types, respectively. Friendly transmission windows are observed around the blue-green wavelengths. Inhomogeneity in pressure, temperature, and salinity can cause water turbulence. Some modeling approaches similar to the atmospheric conditions can be adopted [40,41], but further analytical and experimental

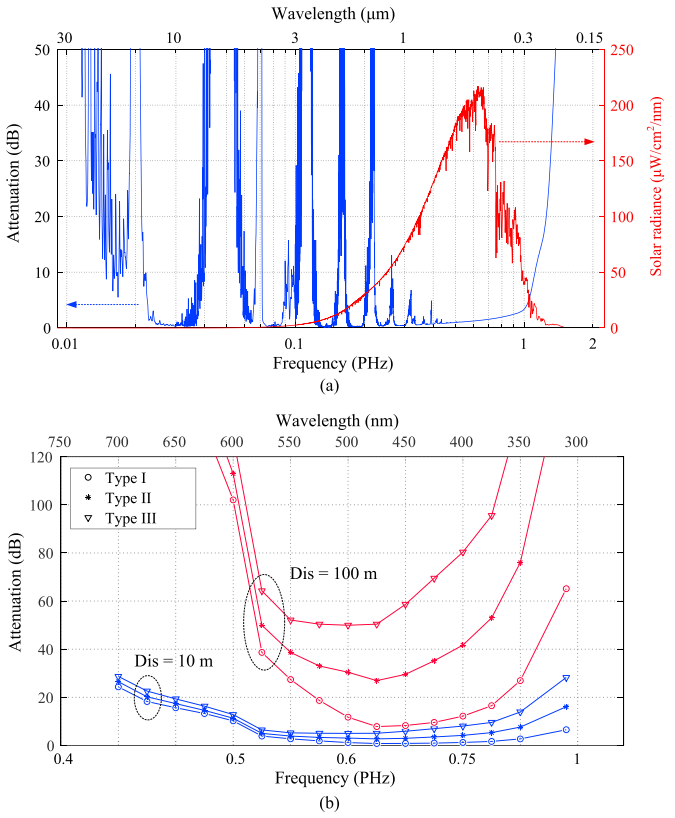

Fig. 4. Channel properties over the wide Petahertz spectrum: (a) outdoor atmospheric attenuation after 1 km propagation distance under solar radiance, (b) underwater attenuation after 10 *m* and 100 *m* propagation distance for three water types.

studies are necessary to fully understand the interaction of the PHz wave with water, marine organisms, bubbles [42], and the air-water interface. Like the outdoor atmospheric channel, layered transmission media and inhomogeneity along the water depth must be integrated into future vertical propagation studies.

3.4.4. *Gaseous-fluid-solid interface channels*

There are scenarios where the PHz wave propagates across the outdoor-indoor interface through glass windows and the outdoor-underwater interface through the water surface. Therefore, reflection, diffusion, and refraction occur at the gaseous-fluid-solid interface. In a practical scenario, it includes air-solid, air-water, and water-solid interfaces. The resultant interface channels alter the PHz wave properties and affect the signal recovery at the Rx.

Air-solid interface channels exist both indoors and outdoors as well as at propagation medium crossings. The PHz wave impinges upon the surface of an object before it is acquired by an Rx. In an indoor environment, interior objects (such as the floor, sidewalls, furniture, machines, and ceiling) are covered by different coating materials, including plaster, gloss paint, wood, aluminum metal, and glass. They incur wavelength-dependent absorption and reflection of an air-solid interface channel, for example, within the IR and VL spectra [43]. Typically, a PHz beam undergoes either diffuse reflection or specular reflection after interaction with the surface, depending on the surface roughness/smoothness. The Lambert-Phong model combines these two effects in a hybrid reflection model [44]. The reflective beam pattern finally governs the received spatial intensity distribution. Similar rules apply to the outdoor air-solid interface channel when the PHz wave interacts with an outdoor object. Furthermore, when the PHz wave penetrates a window, additional refraction occurs due to the refractive indices change of the propagation media on both sides of the interface.

Table 3
Atmospheric transmission windows in 0.01–1.5 PHz.

Index	Spectrum Window
1	0.022–0.035 PHz
2	0.07–0.09 PHz
3	0.12–0.15 PHz
4	0.16–0.20 PHz
5	0.22–0.26 PHz
6	0.27–0.31 PHz
7	0.32–0.38 PHz
8	0.40–0.98 PHz

When a node above the water's surface communicates with an underwater node, it is necessary to establish a communication link penetrating an air-water interface. The over-the-water node may be a satellite, a flying drone, a floating platform, or a terrestrial terminal, while the underwater node may be an unmanned underwater vehicle, a diver, or a sensor node. In such cases, the PHz wave is refracted or partially reflected by the water's surface. In addition to water absorption, ocean waves generate random surface water droplet movements, imposing the unique characteristics of an air-water channel.

Some properties in the VL and UV subbands of a PHz channel have already been studied. For example, the experimental air-water VL channel impulse responses under different water surface conditions were fitted by typical probabilistic distributions in Ref. [45]. Furthermore, the coverage area and VL intensity under turbid water and/or wavy surface conditions were thoroughly analyzed in Ref. [46]. As a recent development, the VLC channel's power decay, temporal spreading, and link coverage characteristics were experimentally reported in Ref. [47]. Finally, the diffused LOS UV communication characteristics and the matching system design were demonstrated across the wavy air-water interface in Ref. [48].

By contrast, when the PHz beam is directed towards a solid object immersed in a watery environment, water-solid interface channel conditions are encountered. For example, an underwater Tx/Rx may communicate with another underwater Tx/Rx indirectly through a reflective surface of an underwater relay node or using the bottom part of a buoy to reflect the PHz signal during its multipath propagation. If an autonomous underwater vehicle having galvanized steel hull is between two communicating divers, the reflected water-solid interface and scattered paths form a full/partial blockage channel [41]. Similarly, an atmospheric water-solid interface in the form of a moist and reflecting surface is created when an object (such as a building, lamp post, or tree trunk) is wetted by rain. In such cases, the associated water-solid interface channels govern the communication performance, which has to be investigated for a variety of scenarios.

Considering the environmental variations along with a direct communication link between an open-air node and an underwater node, or between an outdoor node and an indoor node, it is necessary to select the most appropriate PHz information carrier to match the propagation characteristics in two totally different environments. For example, the same blue/green carrier can be adopted in both the atmosphere and water for the former case, while any PHz carrier with good window-glass penetration capabilities can be considered for the latter case. Different carriers may also be chosen if an assisting relay node is deployed to improve interface-crossing communication. Atmospheric carriers may be changed to IR should an invisible carrier be necessary for enhanced information security; a shorter wavelength can be considered for scattering communication to enhance NLOS operation. In an indoor setting, visible and invisible carriers offer ideal propagation performance over short distances and can be beneficial as long as they impose limited interference on surrounding operators.

3.5. *PetaCom modulation*

Traditional modulation schemes employing different waveforms to drive light sources may be used to strike a spectrum versus power

efficiency trade-off [7,49], such as the simplest On-Off Keying (OOK). Other popular schemes are Pulse Position Modulation (PPM), Pulse Width Modulation (PWM), and Pulse Amplitude Modulation (PAM). Multi-carrier modulation, such as optical Orthogonal Frequency Division Multiplexing (OFDM) [14,50], is capable of increasing data rates in conjunction with high-order Quadrature Amplitude Modulation (QAM) and adaptive power/bit loading. Phase-based modulation applies to a laser source, including Phase-Shift Keying (PSK), differential PSK, and binary/M-ary PSK. Each modulation scheme can be combined with a Multiple-Input Multiple-Output (MIMO) configuration to achieve system performance gains.

Polarization, Spin Angular Momentum (SAM) and Orbital Angular Momentum (OAM), constitute suitable degrees of data modulation freedom in a PetaCom system [14]. Fig. 5 shows a generic block diagram of different modulation schemes. In Polarization-Shift Keying (PolSK), a set of PHz wave polarization states are characterized by three Stokes parameters [51]. Each state is described jointly by the polarization angle and signal phase angle of a high-dimensional constellation. Blocks of information bits are then mapped onto the indices of different polarization states, while signal detection and bit recovery are achieved by a state discriminator. By contrast, OAM modulation maps the information bits to discrete azimuthal phase states of a helical-shaped beam wavefront, namely OAM modes [14]. An OAM beam is constructed by attaching a spiral phase mask to a laser beam, where the mask is generated by a data-controlled hologram using a Spatial Light Modulator (SLM). A set of OAM beams are multiplexed and transmitted via the PHz channel. At the Rx, each de-multiplexed beam is forwarded to an inverse spiral phase mask to recover its phase wavefront and retrieve the information bits.

In addition, both the space and wavelength domains are exploitable. In Optical Spatial Modulation (OSM), multiple transmitters are spatially arranged, but only one light element (e.g., LED) transmits at any given time [9]. The active LED index is determined by the input bit sequence. To recover the bits, the Rx array distinguishes the active LED index for demodulation. Unfortunately, OSM only increases the throughput logarithmically with the number of transmitting elements.

Another modulation design option is to use colors/wavelengths for bit representation. Wavelength-tunable sources are readily available, with wavelengths that can be controlled by the information bits. As such, Wavelength-Shift Keying (WSK) maps the input bits onto the available wavelengths of either wavelength-tunable sources or onto a set of predetermined wavelength sources. The received light passing through optical filters is captured by a set of photodetectors to decode the symbols and generate bits. WSK degenerates to the well-known Color-Shift Keying (CSK) [7] when Red-Green-Blue (RGB) VL carriers relying on RGB LED sources are adopted to increase the data rate [9]. Indeed, in simple tangible terms, the three colors may be viewed as three frequencies in a Frequency-Shift Keying (FSK) detector.

Naturally, the choice of the modulation format has to match the channel characteristics for mitigating the channel impairments, such as the signal-dependent noise [52], interference, and fading. Some of the most compelling applications aim for high-rate or long-distance transmission. High data rates are realizable not only by increasing the electrical bandwidth of the PHz emitters/detectors, but also by exploiting the devices' different degrees of freedom together with high-order and hybrid modulation schemes. For example, CSK increases the number of parallel subchannels [9], OAM offers high modulation order for an information symbol to carry more bits [14], and OFDM mitigates the ISI while increasing the maximum achievable data rate [50]. Similarly, OFDM is also applicable to deal with outdoor and underwater multipath channel ISI due to scattering and reflection. That being said, a long-distance transmission channel may incur severe signal attenuation and lead to very weak received power. Hence, high-gain and high-sensitivity detectors, such as APD or PMT, are preferable in conjunction with a power-efficient modulation scheme. For example, OOK and PPM have been successfully harnessed for underwater communication in the face of high attenuation or turbulence [53,54]. In the presence of channel turbulence, PolSK is preferred to achieve robust performance [51,55], as demonstrated in FSO systems.

3.6. PetaCom system performance

The PetaCom system performance directly depends on the channel quality and system parameters [14], such as the transmit power P_t, wavelength λ, source beam-divergence angle θ_s, Tx/Rx circular lens diameters D_t and D_r, respectively, the communication distance, background radiation, altitude, and visibility *Vis* at sea level. When the wavelength is known, we can approximate the transmit beam angle by λ/D_t.

The four subplots of Fig. 6 show the predicted data rate versus distance in indoor, outdoor terrestrial, space-ground, and underwater scenarios, respectively, all at a targeted Bit-Error Rate (BER) of 3.8×10^{-3}. This BER may typically be reduced to a vanishingly low value by Forward Error Correction (FEC). We assume an optical filter bandwidth of 5 nm, APD responsivity of 0.95 A/W, the internal gain of 30, the temperature of 300 *K*, the load resistance of 50 Ω, the dark current of 0.1 nA, and the excess index of 0.4. Generally, data rates of tens of Tbps are achievable.

Fig. 6a exhibits higher indoor performance sensitivity to beam-divergence than to transmit power upon varying the distance from 1 *m* to 100 *m*. The outdoor terrestrial long-distance performance of Fig. 6b indicates significant sensitivity to the visibility levels as distance increases. The cross-over of different-wavelength curves at certain points in the order of visibility distance for each visibility scenario shows that shorter wavelengths attain higher data rates at short distances, while the trend is reversed for long distances.

Space-ground communication typically utilizes high power and large Rx lenses to improve performance at distances up to 100 km. Fig. 6c presents the space-ground communication data rate curves grouped in terms of Rx lens diameter. Within each group, the longer wavelengths tend to perform better. A data rate of 100 Tbps is achievable at a few kilometers distance and at similar rates as those reported using multiple wavelengths and multiple OAM modes in Ref. [14]. Performance is expected to improve as the technology improves and the beam-width shrinks by a few orders, while the attainable distance may stretch beyond 100 km.

The underwater communication distance is severely limited by water absorption; hence, narrow beams are desirable [56]. The performance curves of Fig. 6d are separated by water types and reflect the clear dominance of attenuation over the geometric loss, starting from 100 m for Type I and about 30 m for Type III. The distance can reach 500 m for Type I, provided that a data rate of 1 kbps is acceptable. It can also be observed that a wavelength of 525 nm is beneficial for Type III water, while 450 nm is beneficial for the other two types [39].

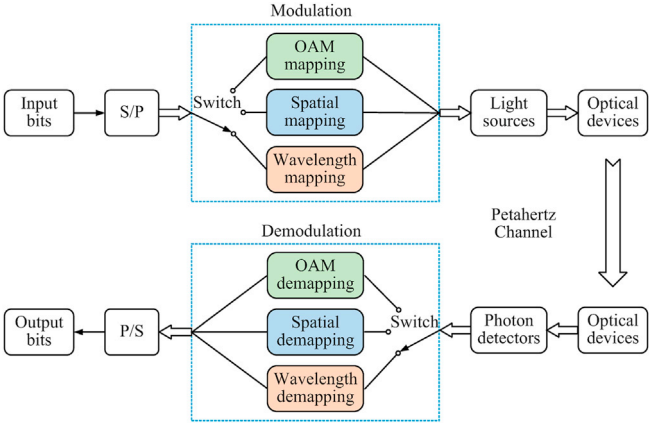

Fig. 5. Block diagram of the OAM, OSM, and WSK modulation schemes.

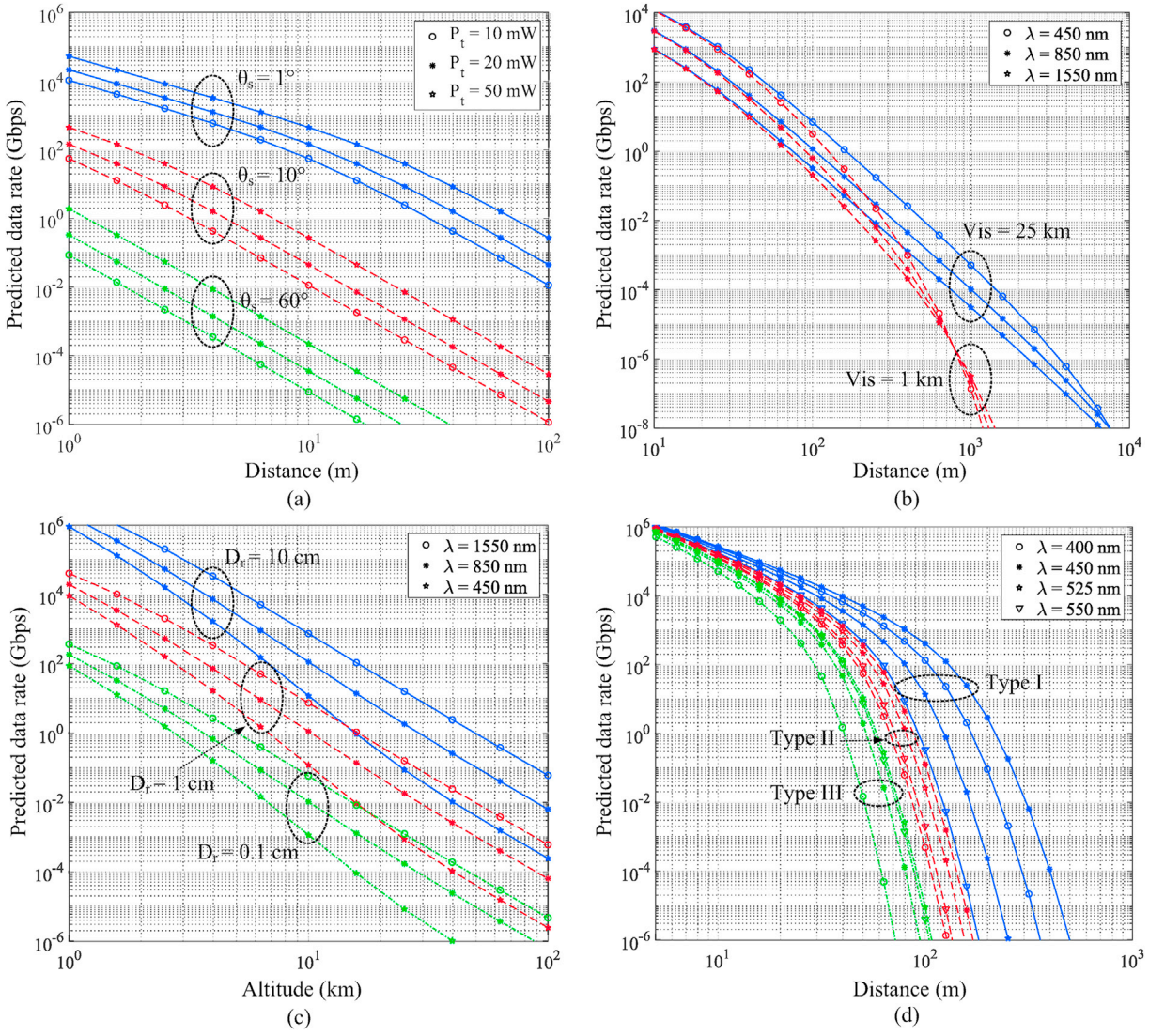

Fig. 6. Predicted OOK-based PetaCom data rate versus distance: (a) indoor performance for different θ_s and P_t, setting $D_r = 1$ mm, $\lambda = 450$ nm; (b) outdoor terrestrial performance for different *Vis* and λ, setting $P_t = 100$ mW, $\theta_s = 1$ mrad, $D_t = 0.1$ mm, $D_r = 1$ mm, typical solar background; (c) space-ground performance for different D_r and λ, setting $P_t = 2$ *W*, $\theta_s = 1$ mrad, exponentially-increasing visibility rate at 0.1/km with altitude from *Vis* = 25 km, and typical solar backgrounds; (d) underwater performance for different water types and λ, setting $P_t = 10$ mW, $\theta_s = 1$ mrad, $D_r = 1$ mm.

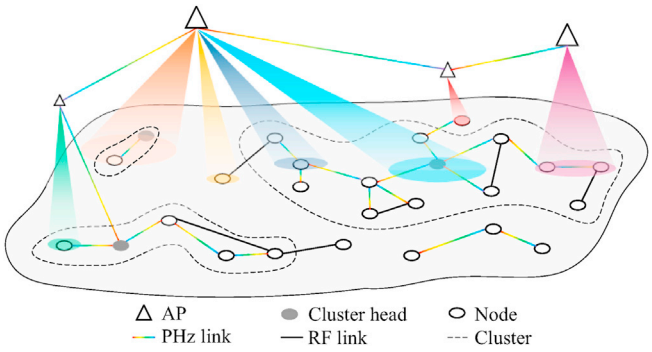

Fig. 7. Multiple access and 3D networking, showing SDMA and WDMA at the APs, replying on node clustering, head node-AP association, non-head node-AP direct communication, and hybrid connections with RF links.

3.7. PetaCom networking

Multiple access allows users to gain simultaneous network access. When realized in domain X, it may be termed as X-Division Multiple Access (XDMA), where X can represent time, frequency, code, beam, momentum, space, and wavelength, resulting in TDMA, FDMA, CDMA, BDMA, MDMA, SDMA, and WDMA, respectively. The latter four are specifically derived from the micro-degree of photon freedom, beam directivity, and carrier separation fine-tuning.

A recently proposed novel BDMA scheme combines the beam and spatial domains for multiple access [57]. Massive optical MIMO transmission from the base station to multiple user terminals is realized through a transmit lens. This scheme asymptotically approaches the maximum attainable sum rate under specific Tx power constraints, and the sum rate increases proportionally with the number of user terminals.

In MDMA, a set of OAM beams possessing different orthogonal OAM modes are multiplexed for transmitting multiple data streams along the same beam axis direction. By contrast, SDMA exploits its tight beam confinement and the resultant spatial reuse whilst avoiding spatial interference. Beam control and angular diversity receivers are routinely exploited. As a further beneficial design alternative, WDMA divides the available bandwidth into different subbands [58], as in optical fiber communications, and each subband is dedicated to a Tx-Rx pair.

The PetaCom network might be expected to pervade the globe in conjunction with fiber, RF, and acoustic networks [59], including long-range or short-range outdoor and indoor scenarios. By its very nature, it is heterogeneous, user-centric, and may be readily integrated with edge computing and edge caching. Fig. 7 illustrates a networking scenario where spatially distributed Access Points (APs) may beneficially harness both spatial and wavelength diversities. Each AP may represent an indoor LED array source, outdoor terrestrial/flying platform, or underwater node. It may have its own beamwidth and beam-direction for unique spatial coverage and have its own wavelength for duplexing and multiple access. The orientations of both the APs and terminals may be exploited for beamforming, user access, neighbor discovery, and network connectivity [60,61]. A subset of nodes forms a cluster, among which one of the most powerful nodes may serve as the cluster head for dynamically coordinating AP association and packet-routing for all other nodes. Naturally, PHz links may also be combined with RF links.

4. Open issues and discussions

Although the aforementioned PetaCom characteristics have their benefits, there are also numerous open challenges, as detailed below.

4.1. Intensity dynamics

An outdoor PetaCom system suffers from solar radiation and other impairments. Furthermore, Tx/Rx mobility and orientation impose signal amplitude fluctuations. A photodetector has a nonlinear Rx characteristic and becomes saturated at a high incident optical power [62,63]. However, indoor link blockage and shadowing, outdoor or underwater NLOS scattering, and long-distance transmission may lead to extremely weak received signals. Hence, suitable detectors capable of capturing wide spectrums and dynamically fluctuating signals are necessary. A tradeoff between the dynamic range and sensitivity has to be struck. Moreover, adaptive Rx architectures have to be conceived.

4.2. Complex interference

Typical sources of contamination are ambient light, device noise, and user interference. The ambient light causes detector saturation and reduces the SNR. A typical photodetector is usually thermal-noise limited, while an APD-based photodetector is generally shot-noise limited. In a dense PetaCom network, the directionality of the PHz beam assists in striking a balance between multiple access interference and coverage, which requires in-depth investigation. Characterizing the complex noise and interference effects is an urgent concern.

4.3. Mobility and coverage

Since the (semi-)directional light source has a limited beamwidth, it is challenging to simultaneously maintain a high rate and a wide coverage area in the mobile scenario. Some tracking techniques have been demonstrated to support moderate mobility [14], while others aim for enhancing the coverage or combining both. For example, an omnidirectional FSO system covers spherical surfaces using numerous inexpensive Tx/Rxs and an auto-configuring circuit. Camera-based visual MIMO sensors are capable of supporting mobility for multiple communicating users. However, radical improvements are required for practical low-medium-high mobility scenarios.

4.4. Diversity techniques

To combat the wavelength-dependent propagation effects, particular attention has to be paid to wavelength diversity. An optical source operating at multiple wavelengths is capable of mitigating the effects of fog, haze, and atmospheric/water turbulence [14]. Wavelength diversity can be combined with sophisticated MIMO configurations and OAM to achieve spatial or angular diversity, albeit at an increased cost and complexity. Joint consideration of the spatial and wavelength diversities under practical channel imperfections is necessary for maximizing the resultant performance gains.

PetaCom systems may suffer from complex distortions, inflicted either by practical optical devices or by imperfect PHz channels, which are difficult to describe by conventional mathematical models. In such cases, artificial intelligence or machine learning techniques are ideal solutions for mitigating imperfections, as suggested in Ref. [64].

5. Conclusion

This article highlighted the potential of the Petahertz band and introduced a Petahertz communication framework for wireless communications, heralding the emerging Petahertz communication era. It further discussed propagation modeling, modulation, system performance evaluation, and multiple access techniques. However, novel photon-based techniques approaching the quantum limits still have to be investigated; hence, colleagues in professional societies are warmly welcomed to join this vibrant community.

Declaration of competing interest

The authors declare that they have no known competing financial interests or personal relationships that could have influenced the work reported in this paper.

Acknowledgements

This work was supported by the Key Program of the National Natural Science Foundation of China (No. 61631018), Key Research Program of Frontier Sciences of CAS (No. QYZDY-SSW-JSC003), and Strategic Priority Research Program of CAS (No. XDA22000000). L. Hanzo would like to acknowledge the financial support of the Engineering and Physical Sciences Research Council projects EP/P034284/1 and EP/P003990/1 (COALESCE) as well as of the European Research Council's Advanced Fellow Grant QuantCom (Grant No. 789028).

References

[1] L. Hanzo, H. Haas, S. Imre, D. O'Brien, M. Rupp, L. Gyongyosi, Wireless myths, realities, and futures: from 3G/4G to optical and quantum wireless, Proc. IEEE 100 (2012) 1853–1888.
[2] E.C. Strinati, S. Barbarossa, J.L. Gonzalez-Jimenez, D. Ktenas, N. Cassiau, L. Maret, C. Dehos, 6G: the next frontier: from holographic messaging to artificial intelligence using subterahertz and visible light communication, IEEE Veh. Technol. Mag. 14 (3) (2019) 42–50.
[3] Z. Zhang, Y. Xiao, Z. Ma, M. Xiao, Z. Ding, X. Lei, G.K. Karagiannidis, P. Fan, 6G wireless networks: vision, requirements, architecture, and key technologies, IEEE Veh. Technol. Mag. 14 (3) (2019) 28–41.
[4] X. You, et al., Towards 6G wireless communication networks: vision, enabling technologies, and new paradigm shifts, Sci. China Inf. Sci. 64 (1) (2021), 110301: 1–110301:74.
[5] 6G White Paper, the next hyper-connected experience for all, 2020, pp. 1–46. https://cdn.codeground.org/nsr/downloads/researchareas/20201201_6G_Vision_web.pdf. Samsung Research.
[6] Z. Ghassemlooy, S. Arnon, M. Uysal, Z. Xu, J. Cheng, Emerging optical wireless communications-Advances and challenges, IEEE J. Sel. Area. Commun. 33 (9) (2015) 1738–1749.
[7] IEEE Standard for Local and metropolitan area networks–Part 15.7, Short-range optical wireless communications, IEEE Std 802.15.7-2018 (2019) 1–407 (Revision of IEEE Std 802.15.7-2011).
[8] Z. Xu, B.M. Sadler, Ultraviolet communications: potential and state-of-the-art, IEEE Commun. Mag. 46 (5) (2008) 67–73.
[9] H. Haas, L. Yin, Y. Wang, C. Chen, What is LiFi? J. Lightwave Technol. 34 (6) (2016) 1533–1544.
[10] M. Uysal, Z. Ghassemlooy, A. Bekkali, A. Kadri, H. Menouar, Visible light communications for vehicular networking: performance study of a V2V system using a measured headlamp beam pattern model, IEEE Veh. Technol. Mag. 10 (4) (2015) 45–53.
[11] K. Cui, G. Chen, Z. Xu, R.D. Roberts, Traffic light to vehicle VLC channel characterization, Appl. Opt. 51 (27) (2012) 6594–6605.
[12] J.M. Kahn, J.R. Barry, Wireless infrared communications, Proc. IEEE 85 (2) (1997) 265–298.
[13] M.A. Khalighi, M. Uysal, Survey on free space optical communication: a communication theory perspective, IEEE Commun. Surveys & Tuts. 16 (4) (2014) 2231–2258.
[14] H. Kaushal, G. Kaddoum, Optical communication in space: challenges and mitigation techniques, IEEE Commun. Surveys & Tuts. 19 (1) (2017) 57–96.
[15] T.A. Tsiftsis, G. Ding, Y. Zou, G.K. Karagiannidis, Z. Han, L. Hanzo, Guest editorial: spectrum sharing and aggregation for future wireless networks, part III, IEEE J. Sel. Area. Commun. 35 (1) (2017) 1–5.
[16] O.P. Luo, et al., IEEE 802.11bb LC usage model document, IEEE 802.11bb, https://mentor.ieee.org/802.11/dcn/18/11-18-1109-05-00bb-lc-usage-model-document.pptx.
[17] V. Jungnickel, et al., Enhance lighting for the internet of things, in: 2019 Global LiFi Congress, (GLC), 2019, pp. 1–6.
[18] J. Yang, D. Li, X. Jiang, S. Chen, L. Hanzo, Enhancing the resilience of low earth orbit remote sensing satellite networks, IEEE Network 34 (4) (2020) 304–311.
[19] D. Menaka, S. Gauni, C.T. Manimegalai, K. Kalimuthu, Vision of IoUT: advances and future trends in optical wireless communication, J. Opt. (2021) 1–14.
[20] M. Jahanbakht, W. Xiang, L. Hanzo, M.R. Azghadi, Internet of underwater things and big marine data analytics–A comprehensive survey, IEEE Commun, Surveys & Tuts. 23 (2) (2021) 904–956.
[21] D. Zou, C. Gong, K. Wang, Z. Xu, Characterization on practical photon counting receiver in optical scattering communication, IEEE Trans. Commun. 67 (3) (2019) 2203–2217.
[22] Z. Jiang, C. Gong, Z. Xu, Achievable rates and signal detection for photon-level photomultiplier receiver based on statistical non-linear model, IEEE Trans. Wireless Commun. 18 (12) (2019) 6015–6029.
[23] W. Liu, Z. Xu, Some practical constraints and solutions for optical camera communication, Phil. Trans. R. Soc. A. 378 (2020) 1–25, 20190191.
[24] W. Huang, P. Tian, Z. Xu, Design and implementation of a real-time CIM-MIMO optical camera communication system, Opt Express 24 (21) (2016) 24567–24579.
[25] T. Yamazato, et al., Image-sensor-based visible light communication for automotive applications, IEEE Commun. Mag. 52 (7) (2014) 88–97.
[26] C.-Y. Wang, et al., Highly efficient lead-free (Bi,Ce)-codoped Cs2Ag0.4Na0.6InCl6 double perovskites for white light-emitting diodes, Chem. Mater. 32 (18) (2020) 7814–7821.
[27] Labsphere, www.labsphere.Com.
[28] W. Liu, D. Zou, Z. Xu, Modeling of optical wireless scattering communication channels over broad spectra, J. Opt. Soc. America A (JOSA A) 32 (3) (2015) 486–490.
[29] J. Ding, Z. Xu, L. Hanzo, Accuracy of the point-source model of a multi-LED array in high-speed visible light communication channel characterization, IEEE Photonics J 7 (4) (2015), 1600714:1–1600714:14.
[30] H. Ding, G. Chen, A. Majumdar, B.M. Sadler, Z. Xu, Modeling of non-line-of-sight ultraviolet scattering channels for communication, IEEE J. Sel. Area. Commun. 27 (9) (2009) 1535–1544.
[31] G. Chen, Z. Xu, H. Ding, B.M. Sadler, Path loss modeling and performance trade-off study for short-range non-line-of-sight ultraviolet communications, Opt Express 17 (5) (2009) 3929–3940.
[32] P. Wang, Z. Xu, Characteristics of ultraviolet scattering and turbulent channels, Opt. Lett. 38 (15) (2013) 2773–2775.
[33] K. Wang, C. Gong, D. Zou, Z. Xu, Turbulence channel modeling and non-parametric estimation for optical wireless scattering communication, J. Lightwave Technol. 35 (13) (2017) 2746–2756.
[34] R.W. Zaki, H.A. Fayed, A.A. Aziz, M.H. Aly, Outdoor visible light communication in intelligent transportation systems: impact of snow and rain, Appl. Sci. 9 (24) (2019), 5453:1–5453:20.
[35] S.A. Zabidi, M.R. Islam, W. Al-Khateeb, A.W. Naji, Analysis of rain effects on terrestrial free space optics based on data measured in tropical climate, IIUM Engineering J 12 (5) (2011) 45–51.
[36] I.T.U.-R.P. Recommendation, Propagation Data Required for the Design of Terrestrial Free-Space Optical Links, International Telecommunication Union Radiocommunication Sector (ITU-R) Std, 1817-1.
[37] E.M. Patterson, J.B. Gillespie, Simplified ultraviolet and visible wavelength atmospheric propagation model, Appl. Opt. 28 (3) (1989) 425–429.
[38] H. Horvath, Atmospheric light absorption–A review, Atmospheric Environment. Part A, General Topics 27 (3) (1993) 293–317.
[39] N.G. Jerlov, Marine Optics, Elsevier Scientific Publishing Company, New York, USA, 1976.
[40] Z. Zeng, S. Fu, H. Zhang, Y. Dong, J. Cheng, A survey of underwater optical wireless communications, IEEE Commun. Surveys & Tuts. 19 (1) (2017) 204–238.
[41] F. Miramirkhani, M. Uysal, Visible light communication channel modeling for underwater environments with blocking and shadowing, IEEE Access 6 (2018) 1082–1090.
[42] D. Chen, J. Wang, S. Li, Z. Xu, Effects of air bubbles on underwater optical wireless communication, Chin. Opt Lett. 17 (10) (2019), 100008:1–100008:6.
[43] F. Miramirkhani, M. Uysal, Channel modeling and characterization for visible light communications, IEEE Photonics J 7 (6) (2015) 1–16.
[44] P.F. Mmbaga, J. Thompson, H. Haas, Performance analysis of indoor diffuse VLC MIMO channels using angular diversity detectors, J. Lightwave Technol. 34 (4) (2016) 1254–1266.
[45] P. Nabavi, A.S. Haq, M. Yuksel, Empirical Modeling and Analysis of Water-To-Air Optical Wireless Communication Channels, IEEE Int. Conf. Commun. Workshops, 2019, pp. 1–6, 2019.
[46] M.S. Islam, M.F. Younis, Analyzing visible light communication through air-water interface, IEEE Access 7 (2019) 123830–123845.
[47] T. Lin, N. Huang, C. Gong, J. Luo, Z. Xu, Preliminary characterization of coverage for water-to-air visible light communication through wavy water surface, IEEE Photonics J 13 (1) (2021) 1–13.
[48] X. Sun, M. Kong, C. Shen, C.H. Kang, T.K. Ng, B.S. Ooi, On the realization of across wavy water-air-interface diffuse-line-of-sight communication based on an ultraviolet emitter, Opt Express 27 (14) (2019), 19635–19649.
[49] Z. Wang, Q. Wang, H. Huang, Z. Xu, Visible Light Communications: Modulation and Signal Processing, Wiley-IEEE Press, USA, 2017.
[50] X. Li, J. Vucic, V. Jungnickel, J. Armstrong, On the capacity of intensity-modulated direct-detection systems and the information rate of ACO-OFDM for indoor optical wireless applications, IEEE Trans. Commun. 60 (3) (2012) 799–809.
[51] Y.Q. Hong, S.K. Han, Polarization-dependent SOA-based PolSK modulation for turbulence-robust FSO communication, Opt Express 29 (10) (2021) 15587–15594.
[52] Q. Gao, S. Hu, C. Gong, Z. Xu, Modulation designs for visible light communications with signal-dependent noise, J. Lightwave Technol. 34 (23) (2016) 5516–5525.
[53] J. Wang, C. Lu, S. Li, Z. Xu, 100 m/500 Mbps underwater optical wireless communication using an NRZ-OOK modulated 520 nm laser diode, Opt Express 27 (9) (2019) 12171–12181.
[54] Y. Baykal, Bit error rate of pulse position modulated optical wireless communication links in oceanic turbulence, J. Opt. Soc. America A (JOSA A) 35 (9) (2018) 1627–1632.
[55] X. Tang, Z. Xu, Z. Ghassemlooy, Coherent polarization modulated transmission through MIMO atmospheric optical turbulence channel, J. Lightwave Technol. 31 (20) (2013) 3221–3228.
[56] W. Liu, Z. Xu, L. Yang, SIMO detection schemes for underwater optical wireless communication under turbulence, Photon. Res. 3 (3) (2015) 48–53.

[57] C. Sun, X. Gao, J. Wang, Z. Ding, X.-G. Xia, Beam domain massive MIMO for optical wireless communications with transmit lens, IEEE Trans. Commun. 67 (3) (2019) 2188–2202.
[58] K. Zhou, C. Gong, Z. Xu, Color planning and intercell interference coordination for multicolor visible light communication networks, J. Lightwave Technol. 35 (22) (2017) 4980–4993.
[59] R. Zhang, J. Wang, Z. Wang, Z. Xu, C. Zhao, L. Hanzo, Visible light communications in heterogeneous networks: paving the way for user-centric design, IEEE Wireless Commun 22 (2) (2015) 8–16.
[60] Y. Li, L. Wang, Z. Xu, S.V. Krishnamurthy, Neighbor discovery for ultraviolet ad hoc networks, IEEE J. Sel. Area. Commun. 29 (10) (2011), 2002–2011.
[61] L. Wang, Y. Li, Z. Xu, On connectivity of wireless ultraviolet networks, J. Opt. Soc. Am. A 28 (10) (2011), 1970–1978.
[62] W. Liu, Z. Xu, APD nonlinearity and its impact on PAM-based visible light communication, IEEE Commun. Lett. 24 (5) (2020) 1057–1061.
[63] W. Liu, Z. Xu, X. Jin, Saturation compensation for visible light communication with off-the-shelf detectors, Opt Express 29 (6) (2021) 9670–9684.
[64] Y. Liu, S. Bi, Z. Shi, L. Hanzo, When machine learning meets big data: a wireless communication perspective, IEEE Veh. Technol. Mag. 15 (1) (2020) 63–72.